Accuracy of three-dimensional proton imaging of an inertial confinement fusion target assessed by Geant4 simulation

Zhuxin Li, Sébastien Incerti, Daniel Beasley, Hao Shen, Shimei Wang, Hervé Seznec, Claire Michelet

Accuracy of three-dimensional proton imaging of an inertial confinement fusion target assessed by Geant4 simulation

Zhuxin Li[a], Sébastien Incerti[a], Daniel Beasley[b], Hao Shen[c], Shimei Wang[c], Hervé Seznec[a], Claire Michelet[a]

[a] CNRS, Université Bordeaux, LP2I Bordeaux , UMR5797, F-33170 Gradignan, France
[b] School of Biomedical Engineering & Imaging Sciences, King's College London, WC2R 2LS, United Kingdom
[c] Key Laboratory of Nuclear Physics and Ion-beam Application, Fudan University, Shanghai 200433, China

Emails:

Zhuxin Li: li@cenbg.in2p3.fr

Claire Michelet: michelet@lp2ib.in2p3.fr

Sébastien Incerti: incerti@lp2ib.in2p3.fr

Daniel Beasley: daniel.beasley@kcl.ac.uk

Hao Shen: haoshen@fudan.edu.cn

Shimei Wang: shimeiwang0819@163.com

Hervé Seznec: seznech@cenbg.in2p3.fr

Corresponding author:

Claire Michelet: michelet@lp2ib.in2p3.fr

Abstract:

The Geant4 toolkit was used to perform benchmark Monte Carlo simulations of proton micro-tomography imaging. A phantom of inertial confinement fusion (ICF) target was designed, based on experimental data. Simulations of STIM (Scanning Transmission Ion Microscopy) and PIXE (Particle Induced X-ray Emission) tomography were performed. Quantitative images were obtained from the TomoRebuild and JPIXET software packages, chosen for their ability to handle large solid angles of X-ray detection. The tomographic images were compared with the original phantom, used as a reference. For STIM-T, the accuracy of the calculated mass density was ≤ 2% for TomoRebuild and ≤ 14% for JPIXET. Corrections of X-ray production cross section and X-ray absorption were tested for the quantification of Ge, used as a dopant in the ICF target. The accuracy on the obtained Ge density was ≤ 2.9% for TomoRebuild and ≤ 6.4% for JPIXET, whereas the error was about 40% without correction.

Keywords:

Geant4 simulation

Proton computed tomography

PIXE tomography

X-ray attenuation

Inertial confinement fusion target

1. Introduction

Particle Induced X-ray Emission Tomography (PIXE-T) in combination with Scanning Transmission Ion Microscopy Tomography (STIM-T) has been used to quantitatively produce the elemental concentration and mass density distributions of microscopic samples of a few tens or hundreds of micrometers in size [1]. These techniques have been applied to the three-dimensional (3D) imaging of microscopic inertial confinement fusion (ICF) targets at Fudan University [2-4]. The ICF target is a small spherical shell, a few hundred micrometers in diameter, made of a polymer of uniform composition and mass density, doped with a high Z element, such as Ge. The dopant's distribution should be uniform as it is intended to avoid laser imprinting and limit hydrodynamic instabilities in ICF ignition. Several 3D imaging experiments have been carried out at Fudan University to quantify the Ge content in ICF targets and check its uniformity. For this, a reconstruction program in MATLAB, using Filtered Back Projection (FBP), has been developed. Two physical phenomena need to be considered when reconstructing PIXE-T data: *i)* Non linear X-ray production (NLXP), caused by the decrease of proton energy in the material, leading to a variation of ionization cross section; *ii)* X-ray absorption (XA) in the material. However, in this reconstruction program, the correction to compensate for X-ray loss does not take into account the solid angle of the detector, which is assumed as a point. Assuming this would require having a small solid angle in experiments, leading to an increase of collecting time. In the present study, we propose to use reconstruction methods able to take into account a large detection solid angle. This would be an advantage, because it could significantly reduce the duration of experiments. At present, two reconstruction software packages, TomoRebuild [5] and JPIXET [6, 7], are able to take into account large solid angles. Their performances have been compared in previous studies on experimental data of biological specimens [5, 8]. The mass densities obtained by the two packages were found similar. However, this was only a rough comparison of one package relative to the other, due to the lack of reference data. In the present study, we define a numerical phantom with given density and composition that will be used as a reference sample, so that accurate tests can be performed. The main purpose of our study is to demonstrate that the different reconstruction methods implemented in TomoRebuild and JPIXET are able to produce accurate quantitative images of ICF targets using a large solid angle.

For this, we propose to use Geant4 as a benchmark [9-11]. Geant4 is the most widely used open source Monte Carlo toolkit to simulate particle-matter interactions. Thanks to its advanced functionalities, Geant4 has been applied to various domains, such as high-energy physics, astrophysics and medical applications. More specifically, Geant4 provides users with complete examples, which are ready-to-use applications. Considering tomographic imaging, the ***doiPET*** so-called "advanced example" is available to simulate positron emission tomography (PET) imaging [12-14]. Specific applications related to PIXE experiments are also provided. For example, the ***xray_fluorescence*** advanced example reproduces various setups for PIXE or XRF experiments [15]. The ***TestEm5*** extended example can be used to test the low energy physics processes in the energy range of a few MeV or below, typically involved in PIXE. For instance, Geant4 was used to simulate X-ray spectra that were compared with experimental spectra obtained from 1.5 MeV proton irradiation of thin foils of Au, Pt, GdF3 and Fe. This comparison showed the ability of Geant4 to predict X-ray spectra for these high-Z samples [16]. A new advanced example for the specific application of 3D imaging of microscopic samples is being developed at CENBG/LP2I Bordeaux. For this, several phantoms dedicated to biological applications were developed, including the upper part of a *Caenorhabditis elegans* nematode derived from experimental data [17, 18]. In the present study, we constructed a numerical ICF target phantom with uniform composition and mass density. Geant4 simulations of STIM-T and PIXE-T were performed on the numerical phantom to generate simulated projection data. The principle of our study is to use these simulated projections as an input to the TomoRebuild and JPIXET software packages, and to compare the reconstructed images to

the original phantom, used as a reference. Our first aim is to compare the quality of the reconstructed images obtained by different reconstruction methods. A second aim is to quantify the accuracy of the two corrections for NLXP and XA effects implemented during the reconstruction process using a large solid angle. For this, a detailed study was performed using TomoRebuild, taking advantage of specific features of Geant4, which gives access to data that are impossible to get from experiments.

2. Materials and methods

2.1. Numerical phantom

Our simulation code was adapted from the ***TestEm5*** "extended example" of Geant4 10.7 version, which is generally used to study the transport of particles through a single layer of material. We modified this code to simulate STIM-T and PIXE-T experiments on more complex objects. The principle of STIM-T is, for each beam position, to measure the residual energy of protons after passing through the object. PIXE-T consists of collecting the X-rays emitted by the atoms of the object. We designed a numerical phantom of an ICF target according to typical samples analyzed at Fudan University [2, 3]. The phantom is a spherical shell with outer radius 196 µm and thickness 25 µm. It is composed of a polymer of uniform composition (stoichiometric ratio C:H = 5:7) and mass density (1.08 g/cm^3), doped with Ge (5% in mass). The mass percentage of each element is indicated in Table 1.

2.2. General set-up for STIM-T and PIXE-T simulations

The phantom is centered at the origin of the Geant4 coordinate system, and placed in a "vacuum" environment. Fig. 1 shows the set-up at the first projection: the proton beam is directed along the x-axis. Just as for real 3D tomography experiments, in the simulation the beam scans over the region of interest (ROI) at a given projection. When it finishes scanning the ROI, it rotates to the next projection and performs the scan again. This procedure is repeated until all projections are simulated. It should be mentioned that in experiments it is the sample that rotates, while in the simulation it is more convenient that the beam rotates, because the positions and directions of the proton beam are easy to parameterize.

2.3. Scan parameters

Scan parameters and number of incident protons are crucial points as the simulations can last several days. The simulations were carried out with a proton beam of 4 MeV (point source). For STIM-T, the entire phantom was scanned over a square, each side of length 500 µm. Similar to typical experimental conditions, a scan of 128 slices × 128 pixels was performed for 100 projections over a range of 180°. As the scan involves ~10^6 beam positions, the scan parameters are defined in a C script, which is used to generate automatically the positions and directions of the proton beam into a macro file. The macro file is then read by Geant4 to run the simulation. Considering the long duration of the simulation, the number of incident protons has been optimized to reduce the calculation time whilst keeping a good precision. For each beam position, 100 protons were used, which is sufficient to give a good quality of image [17]. For PIXE-T simulation, only the central slice was scanned. Indeed, PIXE-T requires much more incident protons than STIM-T because of the low X-ray production cross-sections. A PIXE-T experiment usually requires 10^8 to 10^9 protons for each beam position. If the same conditions were applied in the simulation, it would be unrealistic in terms of duration. In order to minimize the simulation duration while maintaining a good quality of image, we reduced the number of protons to 2×10^6 protons. At the same time, to compensate, we took a very large solid angle for detecting the X-rays. This will be discussed in detail in the section 2.6. Besides, some simulation parameters have been optimized to minimize the duration of the simulation, as explained in the following section.

2.4. Simulation configuration

The simulation configuration was validated in previous studies for steady beam PIXE analysis, based on the Geant4 ***TestEm5*** *e*xample [16-18]. We used the same physics models in our codes for STIM-T and PIXE-T simulations: Livermore models and Bearden's X-ray energy database were applied, as they were found more accurate for simulations at low energy. The tracking step was set to ensure at least 10 effective steps along the particle transportation. In order to minimize computing time, the simulation code was designed for multithreading. In addition, a low energy cutoff 900 eV was applied for the generation of secondary particles including X-rays. Thus, the X-rays were not generated if their energy was below 900 eV. This threshold corresponds to the typical lowest energy limit of most X-ray detectors used in PIXE experiments. Indeed X-ray absorption by the entrance window of the detector becomes too high for detecting X-ray at lower energies. It was also checked that, as expected, this energy limitation did not affect the proton energy loss. This threshold was shown to significantly reduce the simulation time [18]. In these conditions, it took about 5 days for a PIXE-T simulation of 100 projections × 1 slice × 128 pixels on a multicore computer with 100 threads, 2.7 GHz, 768 Gb RAM. If the cutoff was not taken into account, it would take 11 days. For STIM-T of 128 slices, it took about 2.2 hours with the cutoff, while 3 hours without the cutoff.

2.5. Simulation output data

The information required for tomographic reconstruction is recorded and contains: *i)* beam position, *i.e.* indices of projection, slice and pixel; *ii)* energy and momentum of the collected particles, which are transmitted protons for STIM-T and emitted X-rays for PIXE-T. A very practical question in terms of saving data is that a tomography simulation involves ~10^6 beam positions, and many events to collect. To address the problem of large data, we designed a custom ***struct*** variable type to store the information of particles in a compact way. The data are saved in a binary file in append mode. In this way, the output file is about a few megabytes per projection. In addition, remedial measures are implemented in case of interruptions during the simulation, for example power failure. A specific C script was developed to identify where the interruption occurred in order to resume the simulation without need to restart it from the beginning.

One of our objectives is to verify whether the corrections of X-ray attenuation implemented in TomoRebuild are accurate. As these corrections depend on the position of the detector, our tests require the collection of X-rays at different angles. Considering the long duration of a PIXE-T simulation, it would not be realistic to repeat it every time we change the position of the detector. Therefore, the detector is not modelled in the simulation. Instead, we collect the particles of interest in all directions (4π solid angle). The detector is then modeled *after* the simulation by making a selection of the collected particles.

2.6. Selection of simulation output data

The detector is modelled by making a selection of simulation output data *after* finishing the simulation. The selection of events is based on the following conditions: *i)* the angular position of the detector with respect to beam direction; *ii)* the detector solid angle, which depends on the distance of the detector to the sample and the size of entrance window. A C script is used to perform the selection by simply parameterizing the two conditions. In this script, we assume that the detector entrance window is circular, thus, the solid angle is calculated by defining the half apex angle, indicated as $\widehat{AOB}$ in Fig. 2. We chose a configuration similar to the experiments [3]: *i)* For STIM-T, the detector is placed after the sample, *i.e.* the angular position of detector is 0° with respect to beam direction, with a half apex angle of 10.2°; *ii)* For PIXE-T, the detector is placed at 135° with respect to beam direction. However, as mentioned before, only 2×10^6 protons were applied in the present PIXE-T simulation to minimize the duration, leading to a theoretical reduction of the number of detected events. To overcome this difficulty, we chose to take a large half apex angle of 70° in order to obtain sufficient events. In this case, the solid

angle is about 4.134 sr. We should note that such a half apex angle would not be possible in experiments, because the detector would block the oncoming beam.

2.7. Specific simulation conditions for PIXE-T

One of the objectives of the present study is to evaluate the accuracy of the NLXP and XA corrections implemented in the image reconstruction process. For this, we performed PIXE-T simulations in conditions similar to experiments, as explained in the previous sections. We collected the energy and momentum of X-rays going out of the phantom. In order to study independently the effects of NLXP and XA corrections, we took advantage of the flexibility of Geant4, to perform simulations in specific conditions, which are impossible to realize in experiments:

- We collected X-rays in the object, at the position where they are emitted. In this case, the XA effect is excluded.
- We artificially turned off the process of proton energy loss. In this way, the proton energy was kept at the initial energy of 4 MeV along its track in the material. Therefore, the NLXP effect is excluded.

2.8. Voxelized phantoms

Quantitative reconstructions based on STIM-T and PIXE-T simulation results were performed by different reconstruction methods. In order to verify both quantitatively and qualitatively the reconstructed images, we need to compare them with the original images of the phantom used in the simulation, as shown in the Results section. For this, we needed to construct two voxelized phantoms: the first one to compare with STIM-T images; the second one to compare with PIXET-T images. The only difference between the voxelized phantoms used for image analysis is the density values set at each voxel. The density is 1.08 g/cm^3 for STIM-T and 0.054 g/cm^3 for PIXE-T, corresponding to the Ge content. Both voxelized phantoms were made of 128 slices × 128 × 128 voxels (Fig. A1). The voxel size is defined by dividing the scan size (here 500 µm in both y and z directions) by the number of pixels of the scan. One difficulty in building the voxelized phantom is to handle the density distribution for the voxels at the border of object to make sure the density decreases gradually from the object to the vacuum (FA. 1). Indeed, the object is a spherical shell, so its border is not parallel to the grid of voxels. Therefore, we first built a phantom of the same geometry, but with a resolution higher by a factor of 8, *i.e.* 1024 × 1024 ×1024 voxels. Then, the density of each voxel of the final 128 × 128 × 128 voxels phantom was obtained by taking the mean of the 8×8×8 neighbouring voxels of the high-resolution phantom.

2.9. Reconstruction of tomographic images

The tomographic images were reconstructed using two software packages, TomoRebuild [5] and JPIXET [6, 7], performing quantitative reconstructions of STIM-T and PIXET-T images. Their advantage is that they provide NLXP and XA corrections, taking into account a large X-ray detection solid angle. The calculation of the corrections is based on the knowledge of the 3D distribution of mass density obtained from STIM-T. However, the algorithmic approach is different for the two codes:

- For TomoRebuild, the STIM-T reconstruction assumes a global uniform composition in major chemical elements, which is suited to a wide variety of specimens such as ICF targets or biological samples. For this reason, the STIM-T reconstruction is performed independently from PIXE-T. From the 3D STIM-T image, the NLXP and XA corrections for each X-ray emitting element are then computed at each projection angle. They are stored in correction matrices that are incorporated during the iterative process of PIXE-T reconstruction. In this way, each chemical element of interest is reconstructed separately from one another.
- For JPIXET, the reconstruction associates the information from STIM-T and PIXE-T at each iteration and for all elements together. The distributions of element content obtained from PIXE-T are used to calculate the stopping power and X-ray absorption of the material at each iteration.

The element content (major and minor elements) is normalized at each iteration, so that the sum of all mass fractions is 1. In this way, JPIXET can be used for samples that are not homogeneous in composition. However, a special attention should be paid to the reliability of each element content, as an error occurring on a specific chemical element would propagate to the other elements as well. Here, of course, as there is only one element in the PIXE-T data (Ge), we do not have this concern.

The TomoRebuild (TR) software package is developed in C++, at CENBG/LP2I Bordeaux. We used two methods in this study:

- Filtered Back Projection (TR_FBP), based on the exact analytical solution of the continuous description of the tomography problem. FBP is often preferred as a simple and fast method suited for not too noisy data, especially transmission tomography, *i.e.* in our case STIM-T data. Various filters can be applied to smooth the data, at the cost of a slight loss in spatial resolution. Here we present the results using a slight smoothing Hann filter (with 0.5 frequency cut-off).
- Maximum Likelihood Expectation Maximization (TR_MLEM), an iterative method based on a discrete formulation of the tomography problem. MLEM is often used for PIXE-T as a robust algorithm even with noisy and/or incomplete data [6, 19, 20]. The images presented in this study were obtained from 32 iterations, which was the optimal number determined from Normalized Average Absolute Deviation (NAAD) and Normalized Root Mean Squared Deviation (NRMSD) calculations [18].

JPIXET is a GPU (Graphics Processing Units)-accelerated software package, devised at IST/ITN in Lisbon, for the reconstruction of STIM-T and PIXET-T with a choice of iterative algorithms [7], including a GPU version of the Discrete Image Space Reconstruction Algorithm (DISRA) [21], which was used in the present study. The images presented in this study were obtained from 6 iterations.

The reconstruction time does not constitute a severe limitation. For example, for TomoRebuild, using a very basic PC 3.4 GHz, 8 Go RAM, it takes 1 minute to reconstruct a full 3D STIM-T image of 128x128x128 voxels using TR_FBP, and 25 minutes using TR_MLEM. For PIXE-T, it takes 2 minutes for one slice, including the calculation of the NLXP and XA correction matrix, for which the large detection solid angle is modelled by finely discretizing the entrance window of the detector [18]. For JPIXET, both STIM-T and PIXE-T reconstructions are performed together. The reconstruction takes about 11 minutes on a computer 3.7GHz, 32GB RAM with a NVIDIA GeForce GTX 1080 Ti GPU. The images were saved as binary files in “raw data” format, which is suited to most graphics software packages. The images presented here were displayed using the Amira graphic software package (https://www.fei.com/software/amira-3d-for-life-sciences), which is particularly suitable for 3D rendering, and the public domain software ImageJ, developed at the National Institutes of Health (https://imagej.nih.gov/ij).

3. Results

3.1. STIM-T analysis of the mass density

We compared the mass density obtained by different methods, *i.e.* TR_FBP, TR_MLEM and JPIXET. Quantitative reconstruction was performed on 128 slices, we present here the results for the central slice of the phantom (Fig. 3a and A2), which corresponds to the slice simulated in PIXE-T. Firstly, we compared the reconstructed images to the original phantom, used as a reference, by calculating the difference images (Fig. 3c-e):

Difference image = Reconstructed image - Reference image.

Difference images allows one to reveal small reconstruction inaccuracy that would not be clearly visible directly in the reconstructed images, such as reconstruction artifacts appearing as a moiré pattern, or

slight differences at edges for example, as discussed in section 4. Secondly, we compared quantitatively the mass density obtained from the different reconstruction methods (histograms in Fig. 4). For this, we defined four regions of interest (ROI) inside the shell, to check whether the reconstructed mass density was uniform (Fig. 4 ROI 1-4). We also defined two ROI in the background to verify whether the calculated density was close to 0 (Fig. 4 ROI 5-6). ROI 6 was not included in the histogram, because the calculated densities using all methods were very close to 0, as it will be discussed in Section 4.1. Considering each reconstruction method, we observed there was no significant difference between the calculated density of ROI 1-4, thus, we considered the mean density of ROI 1-4 to compare the accuracy of the different reconstruction methods (Table 2).

3.2. PIXE-T analysis of the Ge mass density

3.2.1. Validation of NLXP and XA corrections for TomoRebuild

One of our objectives in the present study is to evaluate the accuracy of the two corrections implemented in TomoRebuild. Fig. 5 shows an example of correction matrices calculated by TomoRebuild (Fig. 5a for NLXP effect, Fig. 5b for XA effect, Fig. 5c for total) for Ge at a specific (arbitrary) projection angle. The total correction factor at a given voxel is calculated as the product of NLXP and XA factors, according to a procedure detailed in a previous publication [18]. The correction matrix is calculated for each projection angle, since the direction of the beam and position of the detector are related to the projection angle. As explained in section 2.7, Geant4 allows one to perform PIXE-T simulations using standard experimental conditions and non-standard conditions, which are impossible to realize in experiments. In this way, we simulate without either the XA or the NLXP effects so that we can validate the corrections calculated by TomoRebuild. The accuracy of reconstructed density values was evaluated in terms of Relative Difference (RD) as follows:

$$RD\ (\%) = \frac{Reconstructed\ value - Reference\ value}{Reference\ value} \times 100$$

For this, four types of PIXE-T data were obtained and compared with the reference data defined for the phantom (Table 3):

1. X-rays were collected at the creation points and the proton energy loss process was turned-off. In this case, NLXP and XA effects were both excluded. Therefore, no correction was required and it was expected that the calculated density should be close to the original density defined in the phantom.
2. X-rays were collected at the exit of the object and the proton energy loss process was turned-off. In this case, only the NLXP effect was excluded. Thus, in the reconstruction process, we applied XA correction to check independently its accuracy. When implementing XA correction, the RD was -1.3 % whereas the error was -3.7% without the correction.
3. X-rays were collected at the creation points but the proton energy loss process was not turned-off. In this case, only the XA effect was excluded. We applied NLXP correction to check independently its accuracy. The accuracy was dramatically improved when NLXP was applied. The RD was -3.3% with the correction, wher[eas the error was 39% without. This shows that NLXP correction is here prominent compared to XA, as expected for a high Z element such as Ge.
4. X-rays were collected at the exit of the object and the proton energy loss process was not turned-off. In this case, both NLXP and XA corrections are required. When implementing both corrections in the reconstruction process, the RD was -2.9%, whereas the error was -40% without any correction.

3.2.2. Ge mass density

Based on the PIXE-T reconstructed images (Fig. A3), we compared the calculated Ge mass density obtained by TR_MLEM and JPIXET. We followed a similar analysis procedure as for STIM-T: we firstly compared the difference images obtained by the two methods (Fig. A4). Then for each method, we compared the calculated Ge mass density in the different ROI (Fig. A5). As for STIM-T, we observed there was no significant difference for Ge mass density in ROI 1-4, thus, we considered the mean density of ROI 1-4 for the comparison of the two reconstruction methods (Table 4).

4. Discussion

4.1. STIM-T analysis

It was observed that JPIXET and TR_MLEM produced, as expected, a density of 0 for the outer vacuum background (Fig. 3c and 3d). This is inherent to these reconstruction methods, as they are iterative methods, for which the calculated densities are constrained to be positive or null. For TR_FBP, the density obtained in the outer background was close to 0 on average, with slight fluctuations between positive and negative density values (moiré pattern visible in Fig. 3b). This behavior was expected for FBP, as an analytical method based on Fourier transform. For the inner background, JPIXET still gave exactly 0 (Fig. 3d and Fig. 4 ROI 5), and for TR methods the densities were close to 0 (Fig. 4 ROI 5). For the shell region (Fig. 4 ROI 1-4), TR methods produced more accurate results than JPIXET, with an accuracy respectively $\leq$ 2.2 % for TR and $\leq$ 14 % for JPIXET (Table 2). Moreover, the density obtained by TR_MLEM was more uniform than JPIXET: the density fluctuations were found about 20% larger with JPIXET than for TR_MLEM (Fig. 4 ROI 1-4). In contrast, the definition of borders was better with JPIXET, whereas a slight density discontinuity was observed for TR methods (Fig. 3b-d). This phenomenon has been already discussed in a previous study, from line profiles on sharp edges [17]. For this reason, we avoided the borders of the shell when we defined the ROI.

4.2. PIXE-T analysis

The results obtained for the distribution of Ge mass density show similarities with STIM-T analysis. For the outer background, both TR_MLEM and JPIXET produced the expected density 0 (Fig. A3 and A4). For the inner background, the density obtained by TR_MLEM was close to 0 (Fig. A5 ROI5), while exactly 0 for JPIXET. For the shell region, TR_MLEM gave a more accurate calculated density (RD: -2.9%) than JPIXET (RD: 6.4%) (Table 4). Moreover, the density obtained by TR_MLEM was more uniform than JPIXET: the density fluctuations were found about 40% larger with JPIXET than for TR_MLEM (Fig. A5 ROI 1-4). However, the definition of borders was better with JPIXET.

5. Conclusion

This study demonstrates the application of the Geant4 simulation toolkit as a benchmark for proton tomography of a typical ICF target. Geant4 simulations produce simulated results that are completely independent of the reconstruction algorithm, so the results can be used to check the accuracy of reconstruction methods. Moreover, our results show the ability of the TomoRebuild and JPIXET software packages to reconstruct quantitative STIM-T and PIXE-T images in the case of large detection solid angle. For both STIM-T and PIXE-T images, TomoRebuild produced more accurate mass density than JPIXET compared to the original phantom used as a reference. However, a particular attention should be paid to the borders of the shell, which were better defined with JPIXET. The present study also validates the NLXP and XA corrections implemented for the compensation of X-ray attenuation. The detailed study of NLXP and XA effects shown from TomoRebuild reconstruction results reveals Geant4's flexibility. Indeed, Geant4 allows one to have access to data that are impossible to obtain in experiments: *i)* X-rays at the position where they are emitted, for which the XA effect is excluded; *ii)*

X-rays generated considering no proton energy loss, for which the production cross section is constant, *i.e.* the NLXP effect is excluded. It is worth mentioning that the Geant4 simulation code that we developed to assess the accuracy of micro-tomography imaging is also suited to other applications. For example, it enables to simulate experiments of "classical" (2D) STIM and PIXE imaging, to check their accuracy. Moreover, Geant4 already contains all physical processes for many types of particles, including ions and X-rays in a wide energy range. Thus, other particle sources can be directly used in our simulation code. A public release of our code is planned in the coming months, in the set of advanced examples of Geant4.

Acknowledgements

This work was financially supported by China Scholarship Council, through a four-year funding (N° 201906680103) of Z. Li's PhD at University of Bordeaux, France, in collaboration with Fudan University. Developments of the reconstruction code were carried out thanks to the financial support of "Mission pour les Initiatives Transverses et Interdisciplinaires" (MITI) of CNRS, in the frame of the "Appel à Projets Interne Inter-Institut 2018", "Simulation Numérique pour le Traitement des Images de tomographie par émission X" – NUMETRIX project. The authors are grateful to P. Desbarats, from Laboratoire Bordelais de Recherche en Informatique (LaBRI), and J.-F. Giovannelli, from Laboratoire de l'Intégration du Matériau au Système (IMS), for their helpful and friendly advice on image reconstruction and analysis techniques. We would also like to thank the Geant4 collaboration, especially Susanna Guatelli, Center for Medical and Radiation Physics, University of Wollongong, Australia, for her technical support and advice as the Geant4 advanced example working group coordinator.

Figure captions

All figures should be in black and white in the printed version

Fig. 1. Schematic view of the phantom in the Geant4 coordinate system. The positions of the beam correspond to the first projection.

Fig. 2. Position of detectors for STIM-T (a) and PIXE-T (b). The $\widehat{AOB}$ angle is used to parameterize the selection of the simulation output data.

Fig. 3. Reconstruction of the 3D STIM-T image of the phantom (a). Analysis of the central slice, corresponding to the slice in PIXE-T simulation, by comparison to the phantom used as a reference. The difference images were obtained using TR_FBP (b), TR_MLEM (c) and JPIXET (d). The same linear color scale was used for all images for comparison purpose.

Fig. 4. Histograms of STIM-T mass densities in ROI-1-5, obtained using different reconstruction methods, compared to the reference density of the original phantom. The error bars correspond to the standard deviation.

Fig. 5. Correction matrices obtained for Ge at the 18^{th} projection (30.6°) arbitrarily taken as an example. Proton energy loss causes NLXP when passing through the sample (a); XA correction depends on the position of the emitting voxels according to the X-ray detector (b). The combination of NLXP and XA gives the final correction matrix (c). A linear grey scale was used to code correction values, from black (maximal correction) to white (1, *i.e.* no correction).

Table captions

Table 1. Composition of the numerical spherical shell phantom used for the STIM-T and PIXE-T simulations.

Table 2. Mean mass density calculated by different reconstruction methods from STIM-T simulation results. The mean density is the mean value of ROI 1-4. The indicated uncertainty only corresponds to the resulting standard deviation.

Table 3. Mean Ge density values obtained with TomoRebuild from four types of PIXE-T data with and without taking into account the NLXP and/or XA corrections, and compared with the reference data. The mean density is the mean value of ROI 1-4. The indicated uncertainty corresponds to standard deviation.

Table 4. Mean Ge density comparison, calculated by different reconstruction methods for PIXE-T simulation results. The mean density is the mean value of ROI 1-4. The indicated uncertainty corresponds to standard deviation.

Appendix - Supplementary data captions

Fig. A1. Voxelized phantom for STIM-T image analysis: 3D view (a) and the central slice (b), corresponding to the slice in the PIXE-T simulation

Fig. A2. Reconstructed STIM-T images using TR_FBP (a), TR_MLEM (b) and JPIXET (c). The images are displayed here with no additional filter (except the han filter used for FBP) nor threshold, so that they can be directly compared to the voxelized version of the original phantom, as shown in Fig. 3.

Fig. A3. Reconstructed PIXE-T images using TR_MLEM (a) and JPIXET (b). The images are displayed here with no additional filter nor threshold, so that they can be directly compared to the voxelized version of the original phantom, as shown in Fig. A4.

Fig. A4. PIXE-T difference images obtained using TR_MLEM (a) and JPIXET (b), compared to the original phantom. The same linear color scale was used for the two images for comparison purpose.

Fig. A5. Histogram of the Ge mass density in ROI 1-5, obtained using different reconstruction methods, compared to the density of the original phantom. The error bars correspond to the standard deviation.

References

[1] Michelet C, Barberet P, Moretto P, Seznec H. Development and applications of STIM- and PIXE-tomography: A review. Nucl Instrum Methods Phys Res B. 2015;363:55-60. https://doi.org/10.1016/j.nimb.2015.08.070.
[2] Lu H, He X, Meng J, Guo N, Rong C, Zhang W, et al. Reconstruction of Ge spatial distribution in ICF target using PIXE-T. Fusion Eng Des. 2016;113:43-50. https://doi.org/10.1016/j.fusengdes.2016.10.006.
[3] Guo N, Lu H, Wang Q, Meng J, Gao D, Zhang Y, et al. A dual-PIXE tomography setup for reconstruction of Germanium in ICF target. Nucl Instrum Methods Phys Res B. 2017;404:162-6. https://doi.org/10.1016/j.nimb.2017.04.041.
[4] Wang S, Yu T, Li J, Xue H, Liu X, Zhang W, et al. Application of silicon drift detector in PIXE tomography system of Fudan University. Nucl Instrum Methods Phys Res B. 2022;512:108-13. https://doi.org/10.1016/j.nimb.2021.12.010.
[5] Michelet C, Barberet P, Desbarats P, Giovannelli J-F, Schou C, Chebil I, et al. An implementation of the NiftyRec medical imaging library for PIXE-tomography reconstruction. Nucl Instrum Methods Phys Res B. 2017;404:131-9. https://doi.org/10.1016/j.nimb.2017.01.067.
[6] Beasley D, Alves L, Barberet P, Bourret S, Devès G, Gordillo N, et al. A comparison of quantitative reconstruction techniques for PIXE-tomography analysis applied to biological samples. Nucl Instrum Methods Phys Res B. 2014;331:248-52. https://doi.org/10.1016/j.nimb.2014.01.028.
[7] Beasley DG, Marques AC, Alves LC, R.C. Fast simulation of Proton Induced X-Ray Emission Tomography using CUDA. Nucl Instrum Methods Phys Res B. 2013;306:109-12. https://doi.org/10.1016/j.nimb.2012.12.053.

[8] Michelet C, Barberet P, Devès G, Bouguelmouna B, Bourret S, Delville M-H, et al. Quantitative reconstruction of PIXE-tomography data for thin samples using GUPIX X-ray emission yields. Nucl Instrum Methods Phys Res B. 2015;348:92-9. https://doi.org/10.1016/j.nimb.2014.11.035.
[9] Allison J, Amako K, Apostolakis J, Arce P, Asai M, Aso T, et al. Recent developments in Geant4. Nucl Instrum Methods Phys Res A. 2016;835:186-225. https://doi.org/10.1016/j.nima.2016.06.125.
[10] Allison J, Amako K, Apostolakis J, Araujo H, Arce Dubois P, Asai M, et al. Geant4 developments and applications. IEEE Trans Nucl Sci. 2006;53:270-8. https://doi.org/10.1109/tns.2006.869826.
[11] Agostinelli S, Allison J, Amako Ka, Apostolakis J, Araujo H, Arce P, et al. GEANT4—a simulation toolkit. Nucl Instrum Methods Phys Res A. 2003;506:250-303. https://doi.org/10.1016/S0168-9002(03)01368-8.
[12] Hirano Y, Nitta M, Inadama N, Nishikido F, Yoshida E, Murayama H, et al. Performance evaluation of a depth-of-interaction detector by use of position-sensitive PMT with a super-bialkali photocathode. Radiol Phys Technol. 2014;7:57-66. https://link.springer.com/article/10.1007/s12194-013-0231-4.
[13] Tsuda T, Murayama H, Kitamura K, Yamaya T, Yoshida E, Omura T, et al. A four-layer depth of interaction detector block for small animal PET. IEEE Trans Nucl Sci. 2004;51:2537-42. https://ieeexplore.ieee.org/document/1344374.
[14] Yoshida E, Tashima H, Shinaji T, Shimizu K, Wakizaka H, Mohammadi A, et al. Development of a whole-body dual ring OpenPET for in-beam PET. IEEE trans radiat plasma med sci. 2017;1:293-300. https://ieeexplore.ieee.org/document/7926423.
[15] Mantero A, Bavdaz B, Owens A, Peacock T, Pia MG, editors. Simulation of X-ray fluorescence and application to planetary astrophysics. 2003 IEEE Nuclear Science Symposium Conference Record (IEEE Cat No03CH37515); 2003 19-25 Oct. 2003. https://ieeexplore.ieee.org/document/1352167.
[16] Incerti S, Barberet P, Dévès G, Michelet C, Francis Z, Ivantchenko V, et al. Comparison of experimental proton-induced fluorescence spectra for a selection of thin high-Z samples with Geant4 Monte Carlo simulations. Nucl Instrum Methods Phys Res B. 2015;358:210-22. https://doi.org/10.1016/j.nimb.2015.06.029.
[17] Michelet C, Li Z, Yang W, Incerti S, Desbarats P, Giovannelli JF, et al. A Geant4 simulation for three-dimensional proton imaging of microscopic samples. Phys Med. 2019;65:172-80. https://doi.org/10.1016/j.ejmp.2019.08.022.
[18] Michelet C, Li Z, Jalenques H, Incerti S, Barberet P, Devès G, et al. A Geant4 simulation of X-ray emission for three-dimensional proton imaging of microscopic samples. Phys Med. 2022;94:85-93. https://doi.org/10.1016/j.ejmp.2021.12.002.
[19] Takahiro S, Akihito Y, Akane K, Takeru O, Yasuyuki I, Yoko T, et al. Particle induced X-ray emission-computed tomography analysis of an adsorbent for extraction chromatography. Nucl Instrum Methods Phys Res B. 2016;371:419-23. https://doi.org/10.1016/j.nimb.2015.09.076.
[20] Ng YK, Orlic I, Liew SC, Loh KK, Tang SM, Osipowicz T, et al. A PIXE micro-tomography experiment using MLEM algorithm. Nucl Instrum Methods Phys Res B. 1997;130:109-12. https://doi.org/10.1016/S0168-583X(97)00303-0.
[21] Sakellariou A, Jamieson DN, Legge GJF. Three-dimensional ion micro-tomography. Nucl Instrum Methods Phys Res B. 2001;181:211-8. https://doi.org/10.1016/S0168-583X(01)00618-8.

Fig. 1

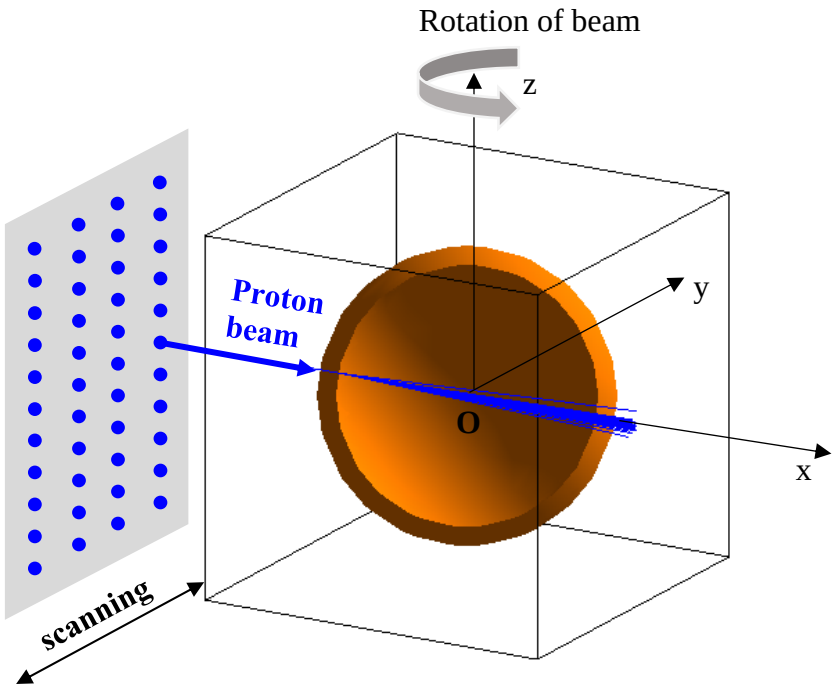
Rotation of beam
z
Proton
beam
y
O
x
scanning

Fig. 2

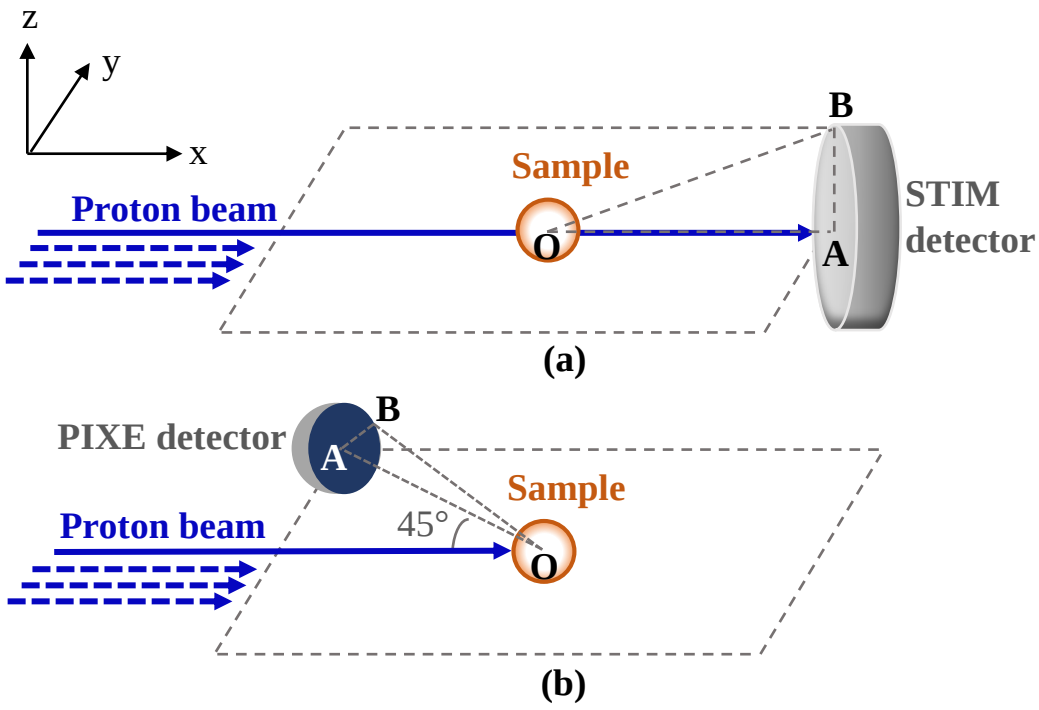
z
y
x
B
Sample
Proton beam
O
A
STIM
detector
(a)
PIXE detector
B
A
Sample
Proton beam
45°
O
(b)

Fig. 3

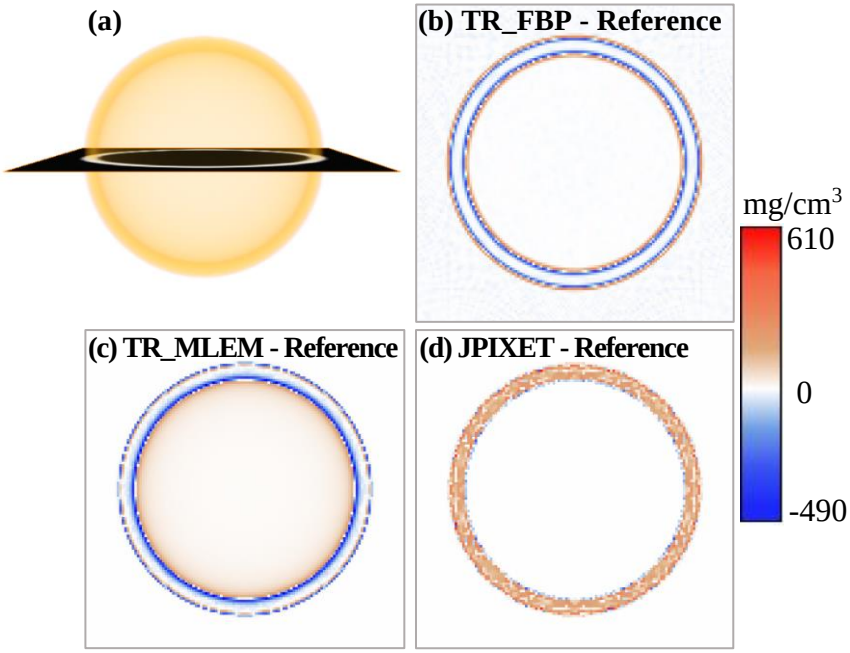
(a)
(b) TR_FBP - Reference
(c) TR_MLEM - Reference
(d) JPIXET - Reference
mg/cm3
610
0
-490

Fig. 4

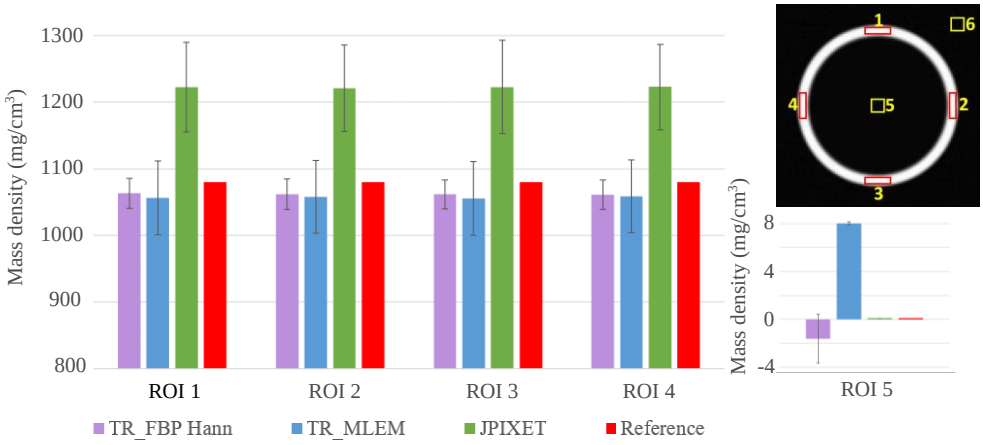
Mass density (mg/cm3)
1300
1200
1100
1000
900
800
ROI 1
ROI 2
ROI 3
ROI 4
TR_FBP Hann
TR_MLEM
JPIXET
Reference
1
2
3
4
5
6
Mass density (mg/cm3)
8
4
0
-4
ROI 5

Fig. 5

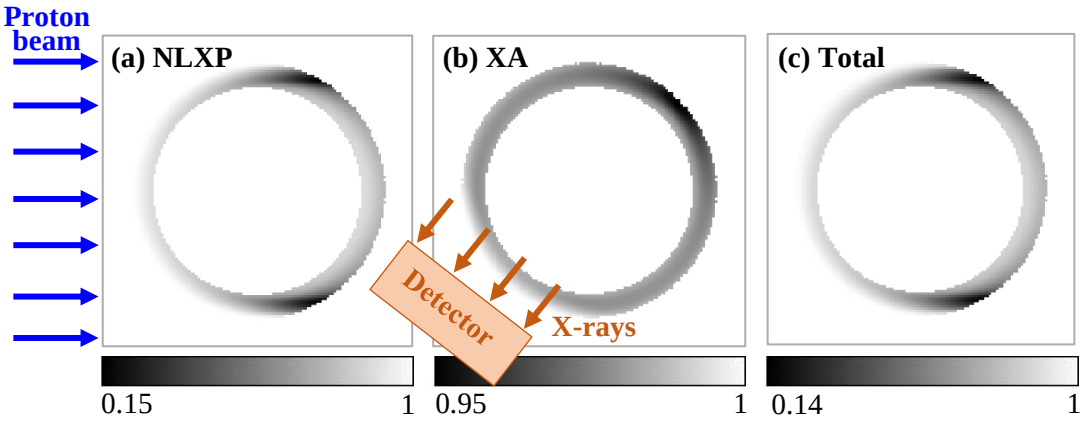

Table 1

Element	Mass percentage (%)
C	85.0
H	10.0
Ge	5.0

Table 2

	Mean mass density (mg/cm^3)	Relative difference (%)
TR_FBP	1062 ± 12	-1.7
TR_MLEM	1057 ± 28	-2.2
JPIXET	1222 ± 34	14
Reference value	**1080**	

Table 3

PIXE-T data type	Correction implemented	Mean Ge mass density (mg/cm^3)	Relative difference (%)
Case 1: both NLXP and XA canceled	No correction required	53.2 ± 2.9	-1.7
Case 2: NLXP canceled	XA correction required and applied	53.4 ± 2.9	-1.3
	Test without XA correction	52.1 ± 2.9	-3.7
Case 3: XA canceled	NLXP required and applied	52.3 ± 3.4	-3.3
	Test without NLXP correction	33.5 ± 3.7	-39
Case 4: NLXP and XA not canceled	Both NLXP and XA required and applied	52.5 ± 3.4	-2.9
	Test without any correction	32.9 ± 3.6	-40
Reference value		**54.0**	

Table 4

	Ge mean density (mg/cm^3)	Relative difference (%)
TR_MLEM	52.5 ± 3.4	-2.9
JPIXET	57.5 ± 4.8	6.4
Reference value	**54.0**	

Appendix Fig. A1

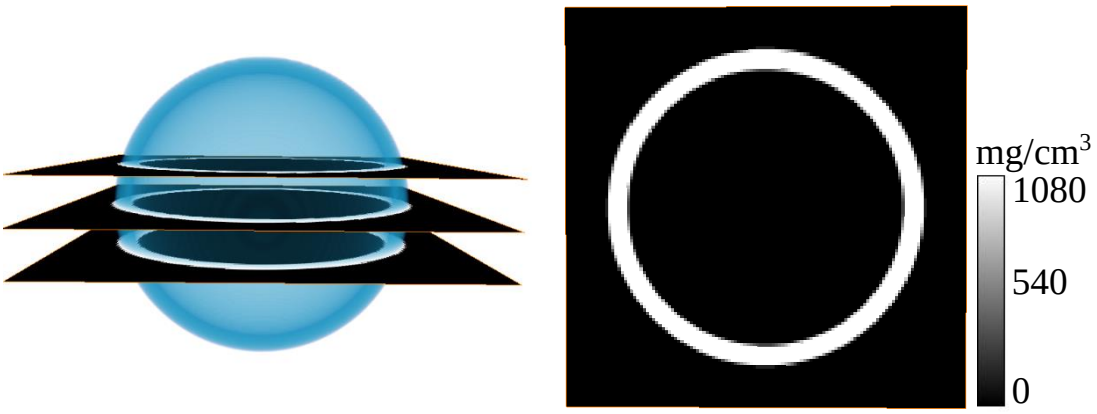

Appendix Fig. A2

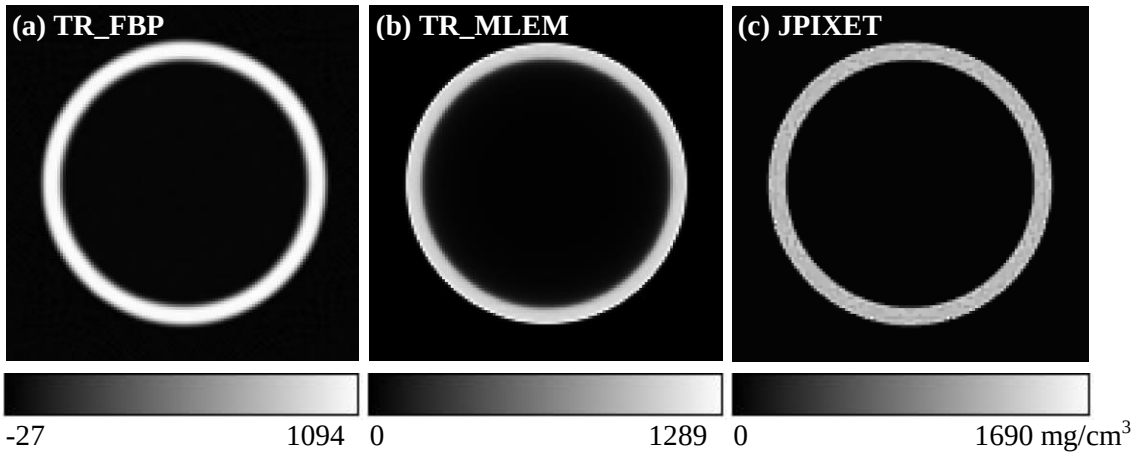

Appendix Fig. A3

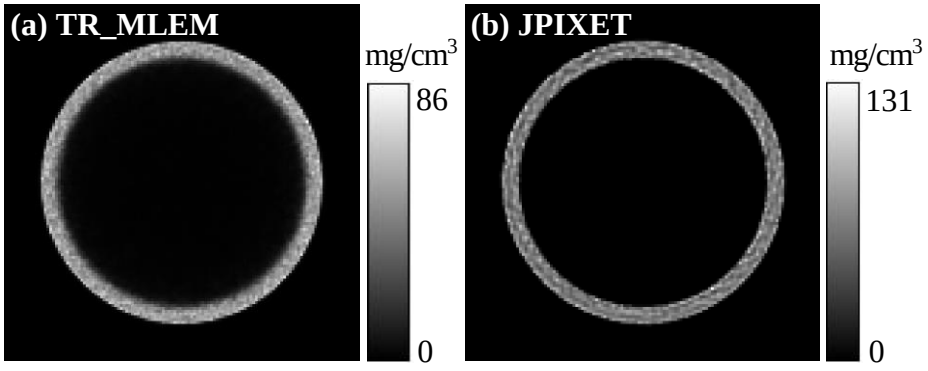

Appendix Fig. A4

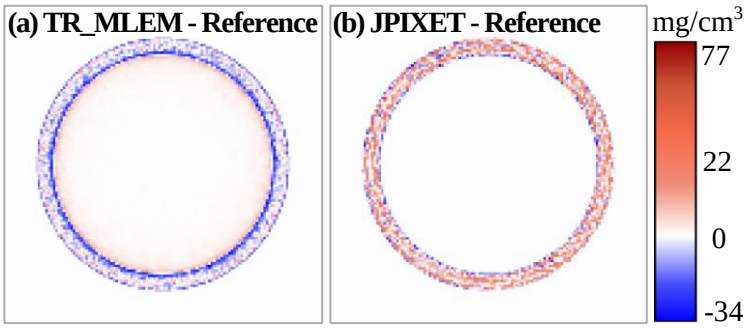

Appendix Fig. A5